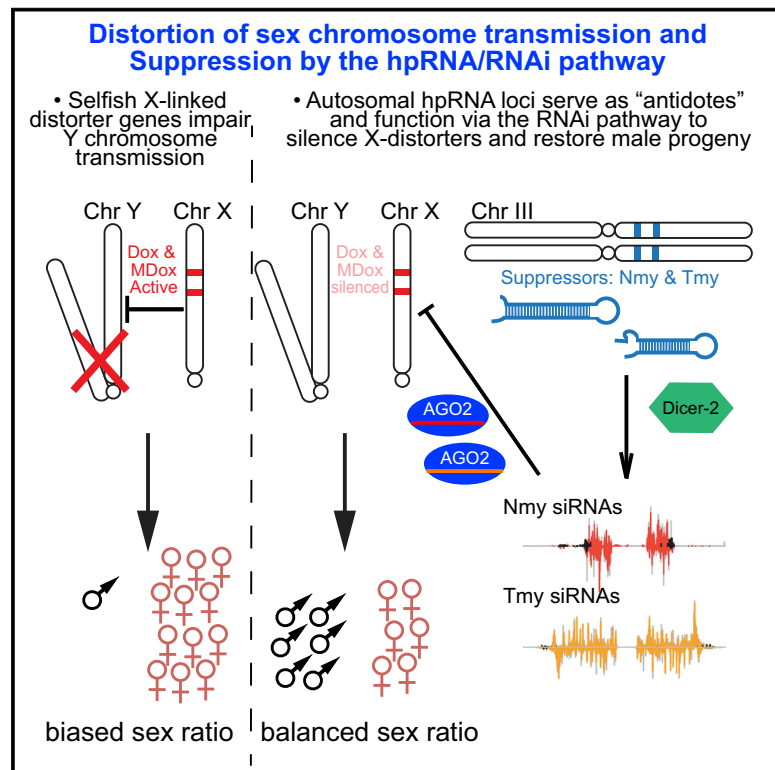


# Developmental Cell

## The hpRNA/RNAi Pathway Is Essential to Resolve Intragenomic Conflict in the *Drosophila* Male Germline

### Graphical Abstract



### Authors

Ching-Jung Lin, Fuqu Hu,  
Raphaelle Dubruille, ..., Peter Smibert,  
Benjamin Loppin, Eric C. Lai

### Correspondence

laie@mskcc.org

### In Brief

Lin and Hu et al. reveal a critical biological usage of RNAi in *Drosophila simulans* to tame meiotic drive systems. Multiple autosomal hairpin-siRNA loci are deployed to suppress X-encoded distorter loci that bias progeny sex ratio. These loci are rapidly evolving and testis restricted, and such intragenomic conflicts may fuel speciation.

### Highlights

- Selfish sex ratio (SR) distorters impede son transmission and must be silenced
- Multiple SR suppressors in *Drosophila simulans* correspond to hairpin RNA-siRNA loci
- Knockout of RNAi pathway derepresses SR drivers and disrupts spermatogenesis
- Rapidly evolving intragenomic conflicts and suppression by RNAi may underlie speciation



# The hpRNA/RNAi Pathway Is Essential to Resolve Intragenomic Conflict in the *Drosophila* Male Germline

Ching-Jung Lin,<sup>1,2,4</sup> Fuqu Hu,<sup>1,4</sup> Raphaelle Dubruille,<sup>3</sup> Jeffrey Vedanayagam,<sup>1</sup> Jiayu Wen,<sup>1,5</sup> Peter Smibert,<sup>1</sup> Benjamin Loppin,<sup>3</sup> and Eric C. Lai<sup>1,6,\*</sup>

<sup>1</sup>Department of Developmental Biology, Sloan-Kettering Institute, 1275 York Ave, Box 252, New York, NY 10065, USA

<sup>2</sup>Weill Graduate School of Medical Sciences, Weill Cornell Medical College, New York, NY 10065, USA

<sup>3</sup>Laboratoire de Biométrie et Biologie Evolutive - UMR5558, Université Claude Bernard Lyon I, 16, rue R. Dubois - Bât. G. Mendel, 69622 Villeurbanne Cedex, France

<sup>4</sup>These authors contributed equally

<sup>5</sup>Present address: Division of Biochemistry and Biomedical Sciences, Research School of Biology, The Australian National University, Canberra, ACT 2601, Australia

<sup>6</sup>Lead Contact

\*Correspondence: laie@mskcc.org

<https://doi.org/10.1016/j.devcel.2018.07.004>

## SUMMARY

Intragenomic conflicts are fueled by rapidly evolving selfish genetic elements, which induce selective pressures to innovate opposing repressive mechanisms. This is patently manifest in sex-ratio (SR) meiotic drive systems, in which distorter and suppressor factors bias and restore equal transmission of X and Y sperm. Here, we reveal that multiple SR suppressors in *Drosophila simulans* (*Nmy* and *Tmy*) encode related hairpin RNAs (hpRNAs), which generate endo-siRNAs that repress the paralogous distorters *Dox* and *MDox*. All components in this drive network are recently evolved and largely testis restricted. To connect SR hpRNA function to the RNAi pathway, we generated *D. simulans* null mutants of *Dcr-2* and *AGO2*. Strikingly, these core RNAi knockouts massively derepress *Dox* and *MDox* and are in fact completely male sterile and exhibit highly defective spermatogenesis. Altogether, our data reveal how the adaptive capacity of hpRNAs is critically deployed to restrict selfish gonadal genetic systems that can exterminate a species.

## INTRODUCTION

RNA interference (RNAi) has long been recognized as a versatile experimental technique, but its endogenous biological utilities have been less tangible. This topic is in principle more accessible in invertebrates, several of which express diverse endogenous siRNAs (endo-siRNAs) via dedicated RNAi machinery that is distinct from the related miRNA pathway (Okamura and Lai, 2008). However, while RNAi mutants in nematodes and flies are compromised at defending viruses (Lu et al., 2005; Wang et al., 2006) and/or transposable elements (TE) (Chung et al.,

2008; Czech et al., 2008; Ghildiyal et al., 2008; Kawamura et al., 2008) and affected by certain extreme environmental perturbations (Lucchetta et al., 2009), RNAi mutants generally exhibit few overt phenotypes under non-sensitized conditions.

We recently uncovered the biological logic of the *Drosophila* hairpin RNA (hpRNA) pathway (Czech et al., 2008; Okamura et al., 2008), in which inverted repeat transcripts preferentially generate endo-siRNAs in the testis and repress specific highly complementary mRNAs (Wen et al., 2015). Although all known hpRNAs are recently evolved, we observed clear evidence for siRNA:target co-evolution, indicating adaptive properties of this regulatory network. While ovaries detectably express hpRNAs and endo-siRNAs, RNAi mutants have relatively little consequence in females. Instead, genetic ablation of RNAi causes spermatogenesis defects and male subfertility (Wen et al., 2015). Nevertheless, *Drosophila melanogaster* RNAi mutant males are fertile, suggesting this species can formally cope without siRNAs, at least within the laboratory setting.

In searching for other manifestations of the hpRNA pathway, we investigated the Winters sex-ratio (SR) system of *Drosophila simulans*. This meiotic drive system is absent from *D. melanogaster* and was born within *D. simulans* subclade species that diverged ~240,000 years ago (Tao et al., 2007a, 2007b). Despite its recent *de novo* appearance, Winters SR factors have profound activities. The *Distorter on X* (*Dox*) promotes X chromosome transmission by suppressing Y-bearing sperm (Tao et al., 2007a), a patently undesirable “wild-type” gene activity that must be silenced in order to maintain the *D. simulans* species. An antidote is encoded by autosomal *Not much yang* (*Nmy*), to which an inverted repeat with a sequence similarity to *Dox* was mapped (Tao et al., 2007b). Signatures consistent with positive selection on Winters factors have been detected within *D. simulans* populations, indicating the system is actively evolving under an “arms-race” scenario (Kingan et al., 2010). While the relationship of *Dox* and *Nmy* was evocative of homology-dependent silencing, there is currently no evidence (1) for molecular species constituting the active output of *Nmy*, (2) that *Nmy* directly or indirectly regulates the expression of *Dox*, (3) whether Winters factors are truly distinct from other



SR systems, or (4) that the RNAi pathway participates in SR control.

In this study, we provide first molecular evidence that hpRNA-siRNAs are functional mediators of son protection in the Winters SR system. Moreover, we reveal that a second, previously uncloned SR suppressor in this species, known as the Durham SR system, involves a previously unknown hpRNA-siRNA locus termed *Tmy*. Although defined as genetically separable SR systems, we show that *Nmy* and *Tmy* are paralogous and have partially overlapping capacity to suppress both *Dox* as well as its progenitor locus *MDox*. To demonstrate a connection to the RNAi pathway, we employed CRISPR/Cas9 to engineer *dcr-2* and *ago2* null mutants in this non-model fruit fly species. Remarkably, these exhibit profound, testis-specific phenotypes that are much more severe than their well-studied *D. melanogaster* counterparts, in that they are completely male sterile due to profound defects in spermatogenesis progression and harbor massive synergistic derepression of *Dox* and *MDox* transcripts, consistent with loss of collaborative suppression by *Nmy* and *Tmy* hpRNAs.

Altogether, these data demonstrate unanticipated complexity of sex-distorting factors and hpRNA-suppressing loci in *D. simulans*, all of which are rapidly evolving and none of which exist in *D. melanogaster*. Thus, RNAi is a key pathway that resolves intragenomic conflict that ensures species survival and fulfills roles in adaptive gonadal gene regulation that are more commonly attributed to the piRNA pathway. This highlights the need to explore a wider range of species to more fully appreciate the evolving functions of germline small RNA pathways.

## RESULTS

### The SR Suppressor *Nmy* Is a *D. simulans* hpRNA Locus

We examined three *nmy* alleles (*SR12-2-7*, *nmy[5-2]*, and *exf*) (Tao et al., 2007b; Yasuno et al., 2013) and validated that homozygous males are fertile but sire extremely female-biased broods at 18°C (Figures 1A and 1B). Thus, loss of this individual locus is sufficient to lead to near population extinction, and these stocks require constant attention for maintenance since balancer chromosomes are not available in *D. simulans*. With this phenotypic confirmation, we sought evidence that *Nmy* might encode an hpRNA. *D. simulans* RNA-seq data indicated the presence of a ~2.8-kb spliced transcript at the *Nmy* locus that is dominantly expressed in testis compared to other tissues (Figure 1C). Notably, analysis of testis small RNA data revealed that abundant small RNAs emanate specifically from the *Nmy* hairpin arms (Figure 1C). Although most small RNAs map to both strands of the highly self-complementary hairpin duplex, we could ascertain the transcribed strand based on the predominance of uniquely mapping RNA-seq reads (Figure 1C).

*Nmy* small RNAs were predominantly ~21 nt RNA in length (Figure 1D) and were expressed at two orders of magnitude higher levels in testes than in ovaries, embryos, or heads (Figure 1E), which are characteristics of *D. melanogaster* hpRNAs (Czech et al., 2008; Okamura et al., 2008). The *exf* mutant deletes most of the *Nmy* transcript including all of the hairpin and thus abrogates possible functions of long and short RNAs. However, *SR12-2-7* only removes a portion of the right hairpin arm and thus is expected to maintain the primary tran-

script (Figure 1C). Notably, sequencing from *SR12-2-7* revealed nearly complete loss of all *Nmy* small RNAs, providing strong evidence that small RNAs are the functional products of *Nmy* (Figure 1C).

### The SR Suppressor *Tmy* Encodes a Newly Recognized *D. simulans* hpRNA

Curiously, we noticed that some *Nmy* small RNAs mapped to another autosomal location. This region contains a gap in the initial release of the *D. simulans* mosaic genome R1.3 and is missing in the *w[501]* R2.02 genome (Figure S1), due to assembly artifacts involving these repetitive regions. The genome assembly challenges are further emphasized by the fact that *Nmy* itself is gapped and placed on the wrong chromosome in R1.3 and remains gapped, although in the correct location, in R2.02 (Figure S1). Notably, the additional autosomal hit of *Nmy*-matching small RNAs resides within a < 100-kb interval to which another SR suppressor, *Too much yin* (*Tmy*), was delimited by introgressions of megabase *Drosophila mauritiana* genomic segments into *D. simulans* (Figure 2A) over 17 years ago (Tao et al., 2001). The causal locus is unknown, and the original introgression lines are no longer extant; *Tmy* was also inferred to cooperate with another factor in the local vicinity to suppress hybrid sterility (Tao et al., 2001).

Fortunately, PacBio sequencing data (A. Larracuente and J.J. Emerson, personal communication) now resolves the *Tmy* genomic region (Figure 2B). Excitingly, it proved to harbor another long inverted repeat that generates small RNAs from its hairpin arms (Figure 2C). This duplex is much more self-complementary than *Nmy*, making it more difficult to assign the transcribed strand; the inverted repeat region is ~3.1 kb in length, with almost identical sequence at the repeat arms and includes a fragmented portion of *DNAREP1* (85 bp) and *INVADER2* (274 bp) TE sequences. In between these two TE sequences, there is a 206-bp satellite DNA sequence, and all three repeat sequences are identical in both arms of the inverted repeat (Figure 2C). Available RNA-seq and small RNA data suggest that the spliced primary *Tmy* transcript is preferentially expressed in testis and does not include the distal flanking repeat elements. Nearly identical sequences of the inverted repeat arms pose a challenge to map paired-end RNA-seq data in this region, as occasionally mate-pair reads get misassigned to a non-proximal inverted repeat arm. Therefore, we treated the reads as unpaired sequences and found the vast majority of reads map to both strands (Figure 2C). However, we recovered distinctive RNA-seq reads from both strands of the hairpin loop region at nearly equal frequency, providing evidence that both *Tmy* genomic strands are transcribed (Figure 2C).

Although we were led to this locus based on a subset of shared siRNAs, the bulk of small RNAs generated by *Nmy* and *Tmy* do not cross-map. In fact, *Tmy* generates a much higher-expressed population of unique siRNAs than does *Nmy* (Figures 1D and 1E), and *nmy* mutants maintain expression of abundant *Tmy*-specific small RNAs (Figure 2C). As with *Nmy*, all the *Tmy*-specific small RNAs are predominantly 21 nt in length and are strongly testis-biased (Figures 1D and 1E). Altogether, these data support the notion that SR phenotypes in *Tmy* introgression lines (Tao et al., 2001) were due to loss of a newly recognized bidirectional hpRNA, which we refer to as *Tmy*.

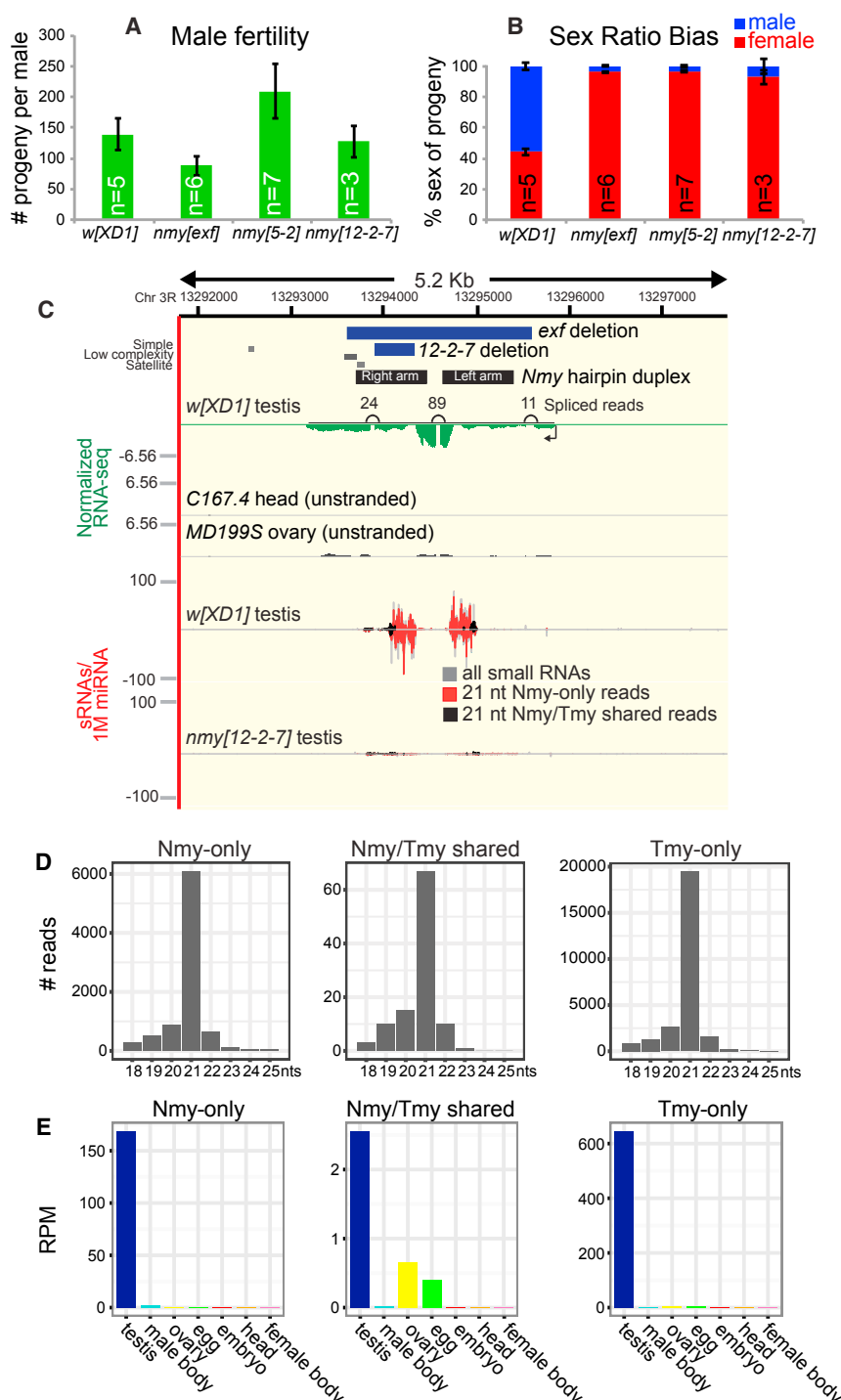


**Figure 1. The *D. simulans* Sex-Ratio Suppressor *Nmy* Encodes a Hairpin RNA**

(A and B) (A) Fertility assay and (B) sex-ratio bias of progeny from *D. simulans* males of control *w[XD1]* and three independent *nmy* mutant alleles. Data are represented as mean  $\pm$  SEM.

(C) Genomics of the *Nmy* locus. Summarizes RNA-seq and small RNA data that define the primary, spliced, testis-biased *Nmy* transcript and small RNAs that emanate specifically from the hairpin arms. These are siRNAs since they are mostly 21 nt (compare colored reads to “all” small RNAs in gray), and *Nmy* reads are missing in *nmy* mutants (red). Note that small RNAs map to both strands, but RNA-seq data define a single strand of transcription. A subset of *Nmy* reads cross-map to another autosomal location that we call *Tmy* (see Figure 2). Most of the cross-mapping reads (black) disappear in *nmy[12-2-7]*, but a subset remains, indicating that they derive from *Tmy*. RNA-seq BigWig tracks represent normalized RNA-seq coverage. Small RNA data were normalized per million miRNAs.

(D) Size distribution of *Nmy* and *Tmy* small RNAs. Small RNAs from *w[XD1]* testis were mapped to the *Tmy* and *Nmy* loci and divided into reads that mapped to one of these loci or that mapped to both loci. All classes of reads showed a 21-nt bias, indicative of siRNA biogenesis.

(E) Expression of *Nmy* and *Tmy* small RNAs across tissues plotted as reads per million (RPM). See also Figures S1 and S2.

SR control, we hypothesize that they may have overlapping activities.

### Nmy and Tmy Have Overlapping Capacity to Regulate Dox and MDox Targets

Our molecular genetic evidence strongly supports the notion that *Nmy* and *Tmy* are hpRNA-siRNA loci (Figure 3A). To provide direct biochemical validation for this, we generated inducible (UAS) expression constructs bearing wild-type *Nmy* and mutant *nmy* isolated from the SR12-2-7 strain. We assayed them with *ub-Gal4* activator in S2 cells from *D. melanogaster*, a non-cognate species that does not encode either of these loci. Northern blotting demonstrated production of small RNAs only from wild-type *Nmy* (Figure 3B). Moreover,  $\beta$ -elimination

increased the mobility of bantam miRNA, but not that of hp-CG4068 and *Nmy* small RNAs, indicating their 3' methylation as expected for siRNAs. We also generated a UAS-*Tmy* construct and identified probes that verified largely distinct small RNA output of *Nmy* and *Tmy* hpRNAs (Figure 3C). Using these probes, we conducted Argonaute immunoprecipitation tests that showed *Nmy* and *Tmy* small RNAs load preferentially into AGO2, in contrast to the miRNA bantam that associates

Remarkably, a single PacBio contig reveals that *Nmy* and *Tmy* are separated by ~2 Mb (Figure 2B), which is reminiscent of the proximity of several homologous *D. melanogaster* hpRNAs into clusters (Wen et al., 2015). The ancestry of *Nmy* and *Tmy* hairpins is further indicated by their extensive homology (Figure 3A), even though the regions that can generate identical siRNAs are limited (Figure S2). Therefore, even though these loci were genetically defined by separable functions in

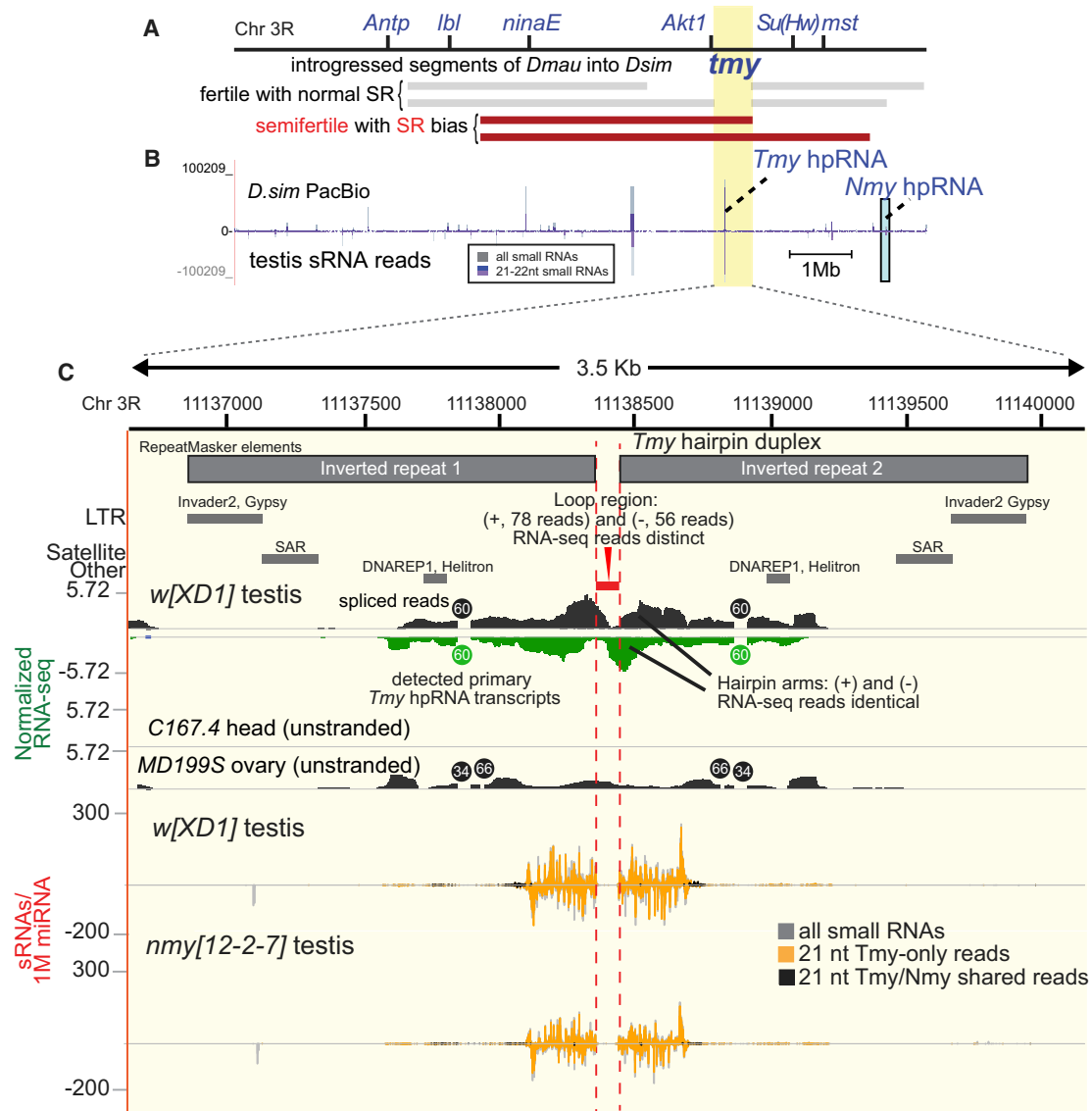


**Figure 2. The *D. simulans* Sex-Ratio Suppressor *Tmy* Encodes an Unannotated hpRNA Related to *Nmy***

(A) Genetic map indicating examples of previously characterized introgression lines of *D. mauritiana* material into *D. simulans* that exhibit sex-ratio (SR) and subfertility defects (summarized from reference [Tao et al., 2001]), which define a minimal genomic interval termed *Tmy*.

(B) This region is misassembled in publicly available genome builds (see Figure S1), but mapping to a PacBio contig reveals that this region contains a bidirectionally transcribed inverted repeat (hpRNA) that is an abundant source of small RNAs. These data correspond to small RNA reads mapped from *D. simulans* testis SRR902009. Raw sRNA mapping density shown along a 14-Mb PacBio contig, with sRNA peak corresponding to *Tmy* hpRNA highlighted in a yellow box, and the *Nmy* hpRNA is shown in a blue box. PacBio contig resolves *Nmy* and *Tmy* hpRNA loci, which are in the same genomic vicinity separated by ~2 Mb on chromosome arm 3R.

(C) Genomics of the *Tmy* region reveals an alternatively spliced transcript that is preferentially expressed in testis. Due to identical inverted repeat sequence at *Tmy*, mate-pairs from paired-end RNA-seq data occasionally get misassigned to a non-proximal repeat arm. Therefore, RNA-seq data were mapped as unpaired, which identifies bidirectional transcription distinguished by uniquely mapping reads at the loop region. RNA-seq BigWig tracks represent normalized RNA-seq coverage. The *Tmy* hairpin yields abundant siRNAs that derive from this locus (“*Tmy*-only” reads, orange), with a subset of reads that cross-map to *Nmy* (“*Tmy*/Nmy-shared reads,” black). Comparison of small RNA data from parallel library constructions from *w[XD1]* and *nmy[12-2-7]* testes confirm that *Tmy* siRNAs are maintained in the absence of *Nmy*. Small RNA data were normalized per million miRNAs. See also Figures S1 and S2.

preferentially with AGO1 (Figure 3D). Thus, *Nmy* and *Tmy* are genuine endo-siRNA loci.

We used RNA-seq data to define the *Dox* transcription unit, which is preferentially expressed in testis compared to several other tissues (Figure S3). Both *Nmy* and *Tmy* hairpins share anti-

sense homology to *Dox* (Figure 4A). However, *Tmy* exhibits a substantial complementary segment to the 5' region of *Dox* that is not shared by *Nmy* (Figure 4A), consistent with the interpretation that it provides an additional activity in SR control. We observe that abundant *Nmy/Tmy* siRNAs map perfectly to

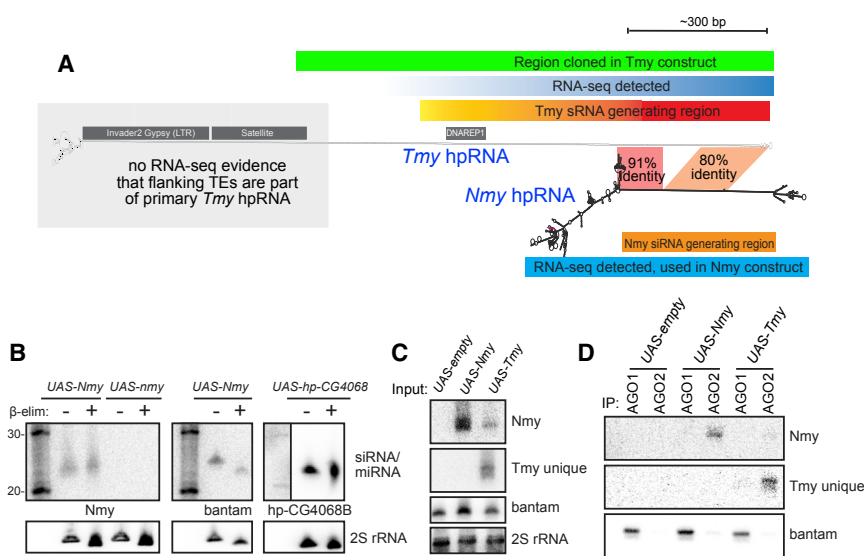


**Figure 3. Biochemical Evidence that Nmy and Tmy hpRNAs Generate Functional siRNAs**

(A) The Tmy and Nmy hpRNAs share homologous segments.

(B) Nmy generates 3'-modified small RNAs that are insensitive to β-elimination. For comparison, the bantam miRNA is sensitive to this treatment, while a known siRNA (hp-CG4068B) from hp-CG4068 is not. A mutant expression construct cloned from the nmy allele SR12-2-7 does not generate small RNAs.

(C) Small RNA products of UAS-Nmy and UAS-Tmy can largely be distinguished using appropriate probe sets. All probes are listed in Table S2.

(D) Nmy and Tmy small RNAs preferentially co-IP with the siRNA effector AGO2, while bantam miRNA associates with AGO1.

*Dox* (Figure S3), indicating that it is under direct control by these hpRNAs. *Dox* is related to an apparent progenitor locus *MDox* (Tao et al., 2007a, 2007b), which is not known to participate in SR distortion but is also located on the X chromosome (Figure S3). RNA-seq data show that *MDox* is also testis-biased and targeted by *Nmy/Tmy* since siRNAs derived from these hpRNAs map perfectly to *MDox* (Figure 4B). We show the overall homology relationships of the SR hpRNA/target network (Figures 4A and 4B) and detailed alignments (Figure S2) and illustrate the region of highest antisense complementarity between *Nmy* and *Tmy* hairpin arms and the transcribed strands of *Dox* and *MDox*, with exemplar *Nmy*-specific, *Tmy*-specific, and shared siRNAs indicated (Figure 4C). In this figure, we emphasize perfect mappers, but note certain siRNAs that map with limited mismatches (e.g., the “blue” *Tmy*-specific siRNAs, Figure 4C); we address these in a following analysis.

Despite substantial homologies across this hpRNA/target network, we note higher antisense matching between *Nmy* and the *Dox* open reading frame (light orange and purple regions, Figure 4A). Correspondingly, many more *Nmy*-specific than *Tmy*-specific siRNAs cross-map to the *Dox* coding sequence, suggesting that *Nmy* might be a dominant regulator of *Dox*. We could confirm that these derive from *Nmy* since they mostly disappeared when sequencing small RNAs from *nmy* [12-2-7]. Nevertheless, we observe that siRNAs still map to *Dox* in *nmy* mutants, and these derive from *Tmy*. These obviously include all *Tmy*-specific siRNAs, including those from the segment complementary to the 5' UTR region of *Dox* that is not shared by *Nmy*. Interestingly, we can also distinguish a population of *Tmy/Nmy*-shared siRNAs that cross-map to the 5' UTR region of *Dox* (colored as dark orange in the model picture of Figure 4A). Their provenance in wild-type would be ambiguous, but a comparison to *nmy* mutant small RNAs allows us to assign that ~19% of apparent *Tmy/Nmy*-shared siRNAs that cross-map to this region actually derive from *Tmy*. Altogether, these data provide molecular evidence that *Tmy* is a likely co-regulator of *Dox*. Similar analyses indicate that *Tmy* likely co-regulates *MDox* (Figure 4B).

To account for targeting more fully, we examined whether there were siRNAs that were complementary to *Dox* or *MDox* splice junctions. Indeed, we could identify a population of such reads and depict their alignments in Figure S4. Because the duplex hpRNA duplex sequence is similar to the target sequence, we recovered *Nmy/Tmy* siRNAs that map both sense and antisense to *Dox/MDox* splice junctions of exons 1/2 and exons 2/3 (Figure S4). Additionally, since full siRNA:target pairing is not needed for AGO2-mediated target regulation (Haley and Zamore, 2004), the impact of *Nmy/Tmy* regulation on *Dox/MDox* may extend beyond perfect matching (see Figure 4C). Although the rules for siRNA targeting are not fully known, we implemented relaxed mapping with up to 3 mismatches, and recovered a substantially larger pool of siRNAs that could target *Dox* and *MDox* (Figure S4). We also explored how many mismatched siRNAs exhibited perfect pairing to an extended seed region that is continuous with the cleavage site (from siRNA nts 2-13), and observed that many siRNAs satisfy this criterion (Figure S4). However, the majority of siRNAs match perfectly to these targets.

To provide experimental support for these regulatory relationships, we tested the sufficiency of *Nmy* and *Tmy* hpRNA expression constructs for their ability to suppress luciferase sensors bearing the co-targeted regions of *Dox* or *MDox* in S2 cells. We compared these to a *nmy*[12-2-7] mutant construct or a *tmy* mutant bearing only one hairpin arm, as well as to empty or non-cognate (*hpRNA1*) constructs. We observed specific repression of both targets by both wild-type *D. simulans* hpRNAs, while mutant *nmy* and *tmy* constructs were non-functional (Figure 4D). Overall, these findings support the notion that a network of siRNA-generating loci mediates SR control in *D. simulans*, working to suppress multiple distorts loci.

We sought *in vivo* evidence for hpRNA-mediated target suppression. Although *Dox* and *MDox* share substantial homology, we were able to design unique primer pairs that amplify specific transcript amplicons (Figure S2). Using biologically replicate testis samples from the three independent alleles of *nmy*, we observed strong upregulation of both *Dox* (~10-fold, Figure 5A) and *MDox* (3- to 8-fold, Figure 5B). This constitutes the first

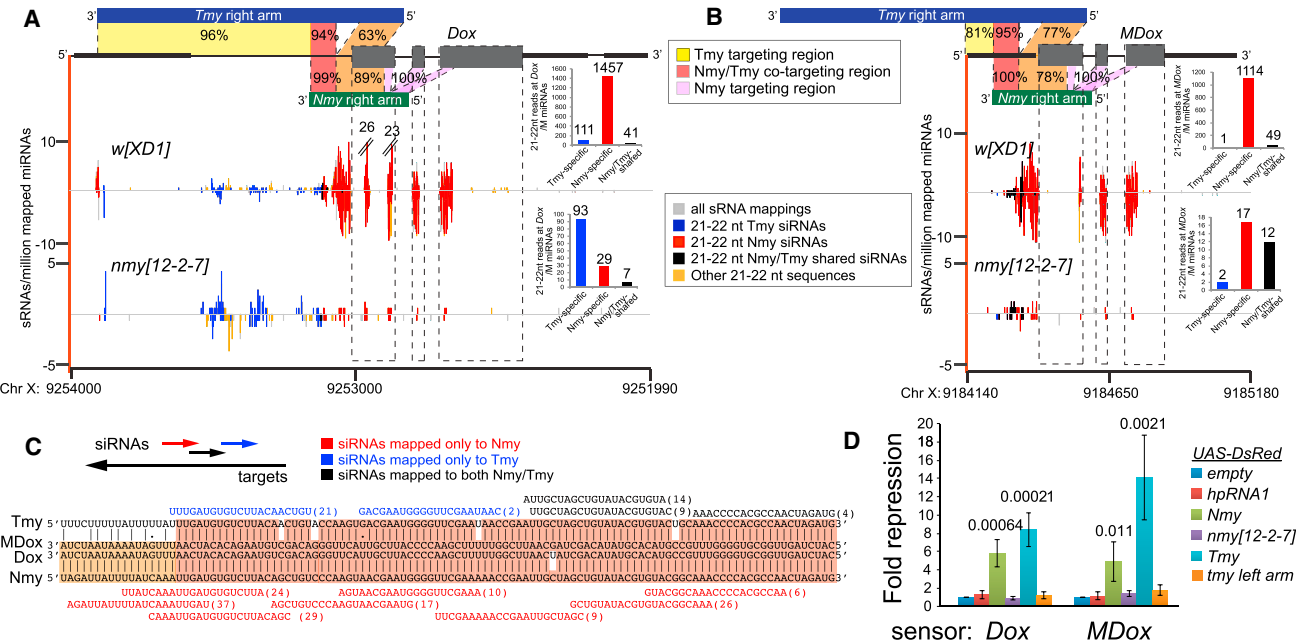


**Figure 4. *Nmy* and *Tmy* hpRNAs Have Partially Overlapping Capacity to Target a Network of Sex-Ratio Distorter Genes**

(A and B) Homology relationships among complementary arms of *Tmy*/*Nmy* with the transcribed strands of *Dox* (A) and *MDox* (B). Note that *Nmy* and *Tmy* bear segments of antisense co-targeting to both *Dox* and *MDox* but that *Tmy* has additional extensive complementarity to the 5' region of *Dox* that is not shared with *Nmy* (A). The relative numbers of *Nmy*-derived siRNAs that map perfectly to *Dox* and *MDox* are higher than with *Tmy*, suggesting it is a primary endogenous suppressor of these factors. Still, substantial perfect targeting by *Tmy*-derived siRNAs to *Dox* and *MDox* remains in *nmy[12-2-7]* testis, consistent with the notion that *Tmy* plays an overlapping role in their suppression.

(C) Alignment of illustrative hairpin arm regions of *Tmy* and *Nmy* that exhibit extensive antisense complementarity to the *Dox* and *MDox* target genes. Selected individual siRNAs that map perfectly to *Tmy* (blue), *Nmy* (red), or both hpRNAs (black) are indicated.

(D) Both *Tmy* and *Nmy* hpRNAs suppress both *Dox* and *MDox* sensors, while mutant *Nmy* and *Tmy* constructs and non-cognate *hpRNA1* construct lack activity on these sensors. Unpaired t tests were used to calculate statistical significance. Three biological replicates were combined for analysis and data are represented as mean  $\pm$  SD. See also Figures S3 and S4.

direct evidence for endogenous deregulation of either target loci in *nmy* hpRNA mutants, conditions associated with strong depletion of male progeny (Figure 1A).

#### *D. simulans* Core RNAi Pathway Mutants Exhibit Profound Male-Specific Defects

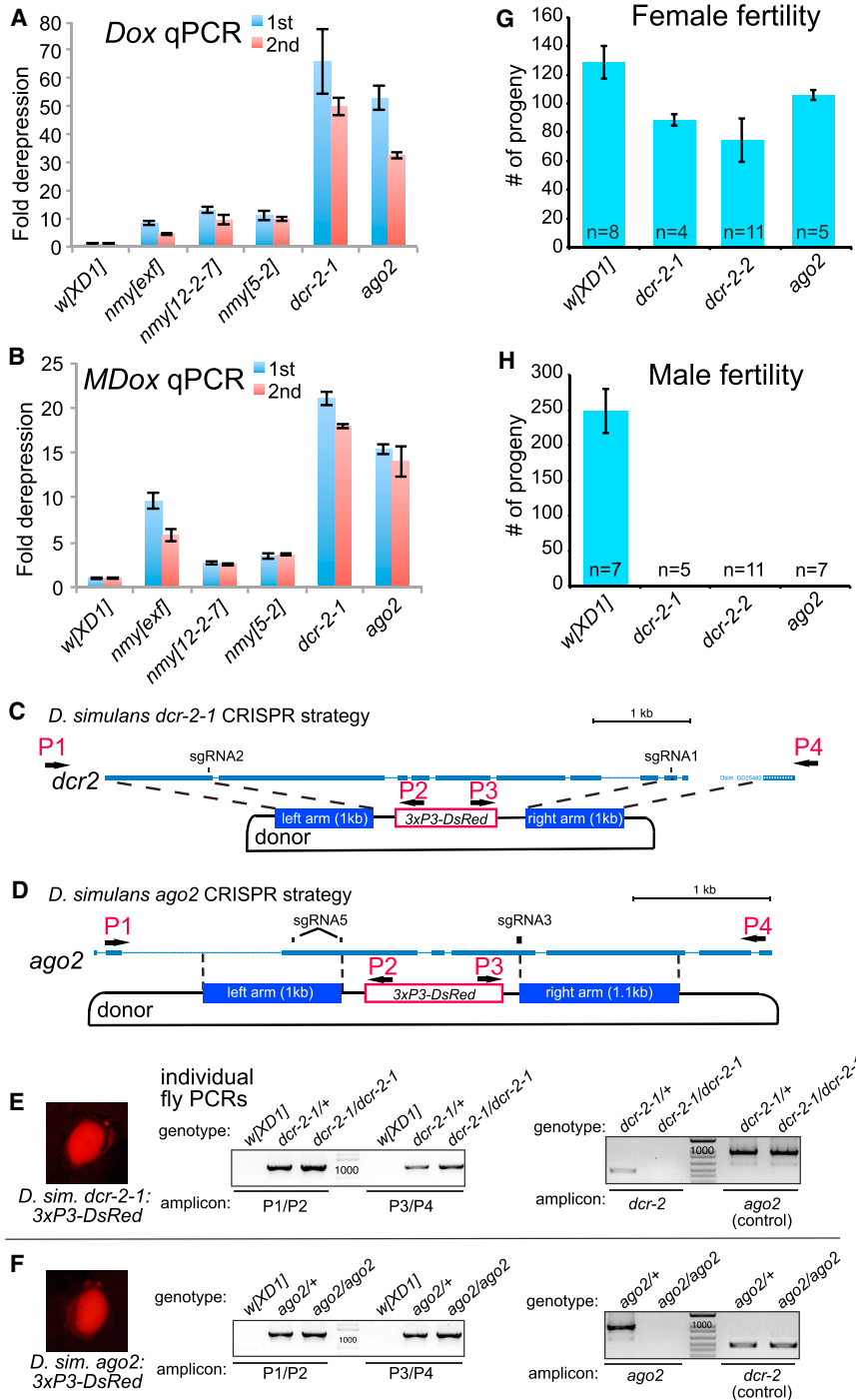
A rigorous connection of *Nmy* and *Tmy* functions to the RNAi pathway requires *in vivo* genetic evidence. We exploited CRISPR-Cas9 engineering to delete the core RNAi factors *dcr-2* and *ago2* and replace them with 3xP3-*DsRed* (Figures 5C and 5D); we used two donors to delete different regions of *dcr-2* (Figure S5). For all experiments, we recovered multiple founders that expressed *DsRed*, passed this through the germline and were validated as bearing on-target gene replacement by hybrid PCRs on both flanks and deleted the target genes (Figures S5 and S6). Because *D. simulans* lacks balancer chromosomes and eye fluorescence could be used to track flies bearing a replacement allele (Figures 5E and 5F) but was not fully reliable to distinguish heterozygotes from homozygotes, we confirmed mutants based on individual fly genotyping for experiments (Figures 5E and 5F). These analyses showed that RNAi is dispensable for viability in *D. simulans*, as is the case in *D. melanogaster*.

These RNAi mutants maintained female fertility that was only slightly lower than that of control *w[XD1]* background used for CRISPR mutagenesis (Figure 5G). In sharp contrast, males of

multiple independent alleles of all three *D. simulans* *dcr-2* and *ago2* mutants assayed were completely sterile (Figure 5H). Thus, RNAi is of greater overt phenotypic impact in this non-model fruit fly than in *D. melanogaster*. Moreover, we note that *D. melanogaster* mutants of the central primary piRNA effector *P element-induced wimpy testis (piwi)* are male fertile (Ku et al., 2016). Therefore, in terms of species propagation, RNAi is more critical for *D. simulans* males than primary piRNAs are for *D. melanogaster* males.

We performed cytological analyses to understand the basis of male infertility in *D. simulans* RNAi mutants, and to compare this to *nmy* mutants, which are fertile but sex-biased (Figure 1A). Indeed, we observed severe disruptions in spermatogenesis that were phenocopied by both *dcr-2* mutants as well as *ago2* mutants, indicating common biological consequences to loss of RNAi function *in vivo* (Figures 6A–6D).

We investigate the basis of defective spermatogenesis in detail. We first analyzed the testis apical tip where the stem cell niche resides; this appeared normal in *nmy* and RNAi mutants (Figures 6E–6H). However, while the rest of the testis was normal in *nmy*, RNAi mutants exhibited severe disorganization. As normal spermatid cysts mature to generate individual sperm, they extrude their cytoplasm in a coordinated fashion via actin-rich cones that are collectively referred to as individualization complexes (ICs), eventually forming waste bags (WBs) (Figure 6).



While both structures are present in *nmy* (Figure 6J), no ICs or WBs can be observed in any of the RNAi mutants, and only scattered actin cones can be seen (Figures 6K and 6L).

Closer examination of spermatid nuclei was informative. After wild-type meiosis, the cysts of 64 spermatid nuclei that mature in synchrony were visible (Figure 6M). In *nmy* mutants, we observed substantial post-meiotic nuclei with aberrant morphologies that likely reflect Y-bearing spermatids (Figure 6N, arrowheads). The phenotype of RNAi mutants was more severe, as

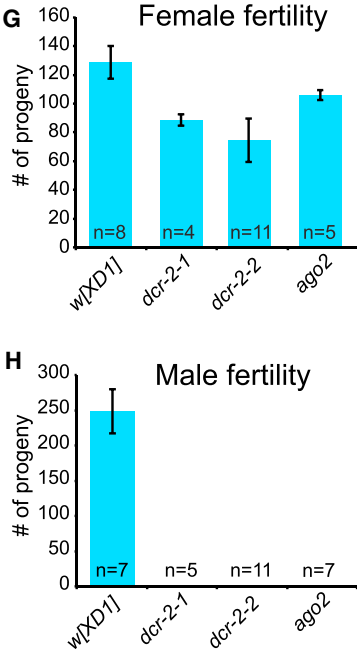


**Figure 5. *Nmy* and *Tmy* hpRNAs Suppress SR Distorters via a Testis-Directed RNA Pathway in *D. simulans***

(A and B) Testis qPCR tests of *Dox* (A) and *MDox* (B) show strong derepression in testis of three independent *nmy* alleles, and massive derepression in null alleles of RNAi factors *dcr-2* and *ago2*. Data are represented as mean  $\pm$  SD.

(C and D) Strategy to generate deletion alleles of *D. simulans* *dcr-2* and *ago2* by replacing their coding regions with 3xP3-DsRed.

(E and F) Validation of DsRed+ *dcr-2* and *ago2* mutants, with individual fly PCR demonstration of on-target knockin of the donor cassette using both left (P1/P2) and right arm (P3/P4) amplicons, and absence of *dcr-2* or *ago2* amplicon and presence of control amplicon.

(G) Null alleles of *dcr-2* and *ago2* show only mild effects on female fertility; *dcr-2<sup>-1</sup>* and *dcr-2<sup>-2</sup>* are different deletions of *dcr-2* (see also Figures S5 and S6). Data are represented as mean  $\pm$  SEM.

(H) Null alleles of *dcr-2* and *ago2* are absolutely male sterile. Data are represented as mean  $\pm$  SEM.

they exhibit aberrant meiotic divisions, which produce spermatid nuclei that are abnormally shaped, frequently connected by chromatin threads, and scattered. Moreover, histones remained associated, implying failure of protamine replacement (Figures 6O and 6P). In the end, *nmy* mutants exhibit a moderate reduction of mature sperm in the seminal vesicle, but *dcr-2* and *ago2* mutants fail to generate any mature sperm (Figures 6Q–6T). We observed a similar suite of phenotypes in the other *dcr-2* deletion allele but not in heterozygotes (Figure S7). Thus, loss of RNAi is much more severe than loss of the single hpRNA *Nmy*.

The complete spermatogenesis defect and male sterility of *D. simulans* RNAi mutants prevented us from assessing SR bias in their progeny and potentially hints at broader intragenomic conflicts that involve *Tmy* (i.e., hybrid sterility [Tao et al., 2001]). We explored different strategies to obtain RNAi mutant progeny (e.g., by altering temperature or by aging), but these did not bypass sterility under any conditions tested; progeny of *dcr-2*/

*ago2* double heterozygotes also exhibited normal SR. Nevertheless, we observed a profound and common molecular phenotype that links RNAi mutants to *nmy* mutants with respect to SR suppression. In particular, quantitative PCR (qPCR) analysis revealed massive derepression of *Dox* (~50-fold) and *MDox* (~15- to 20-fold) transcripts in both *dcr-2* and *ago2* mutant testes, levels that were much greater than any *nmy* mutant background (Figures 5A and 5B). These data affirm that *MDox* is likely a functional distorter gene, which has not previously been

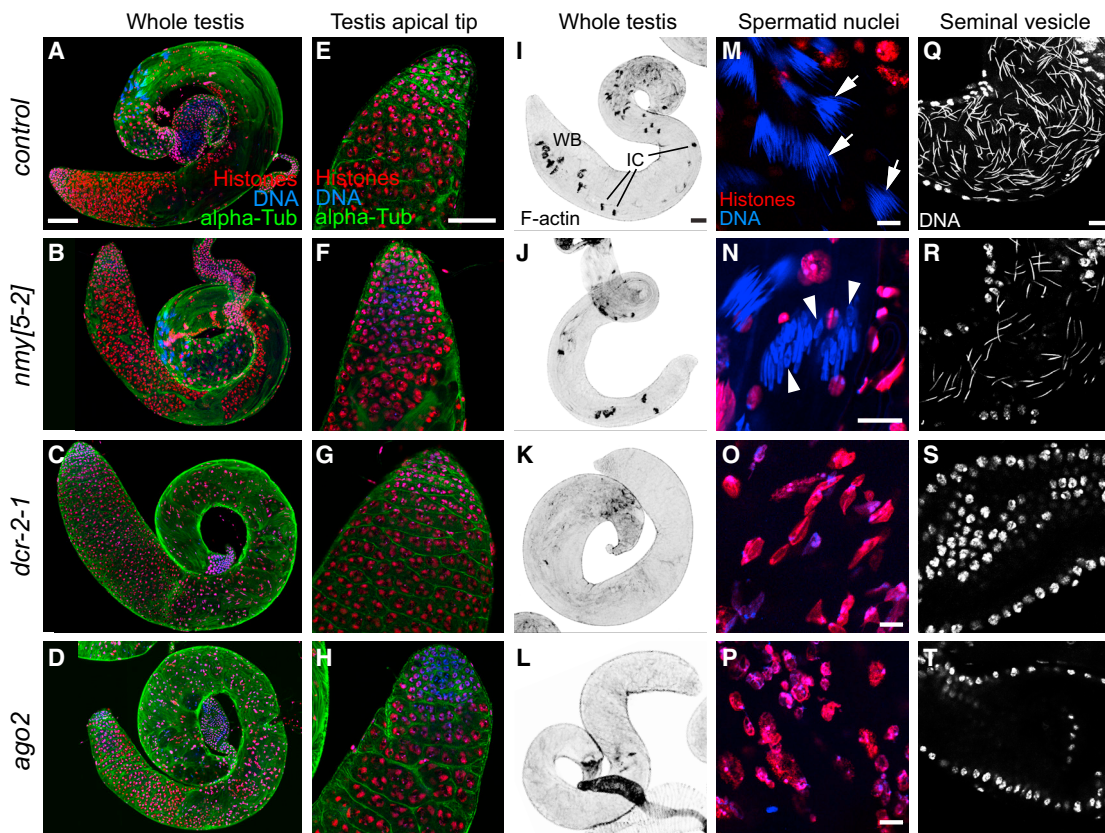


**Figure 6. Abnormal Spermatogenesis in hpRNA/RNAi Mutants**

(A–H) Whole testes stained for DNA (blue), histones (red), and alpha-tubulin (green), showing that the normal pattern of spermatogenesis in control (A) is present in *nmy* (B) but severely disrupted in RNAi mutants *dcr-2* (C) and *ago2* (D). Scale bar represents 100  $\mu$ m. (E–H) The apical tip of the testes containing the stem cell hub in wild-type (E) appears normal in *nmy[5-2]* (F), *dcr-2* (G), and *ago2* (H) mutants. Scale bar represents 50  $\mu$ m.

(I–L) Whole testis stained for F-actin to highlight individualization complexes (IC) that separate spermatids into individual cells to form waste bags (WBs). These actin structures found in control (I) and *nmy* (J) are completely absent in *dcr-2* (K) and *ago2* (L) mutants. Scale bar represents 50  $\mu$ m.

(M–P) Close ups of post-meiotic spermatid nuclei. (M) In control testes, cysts of 64 interconnected spermatid nuclei after the histone-to-protamine transition are visible (arrows). (N) Close-up of *nmy* cysts that have completed histone-to-protamine transition. Two types of nuclei are visible: ones with normal canoe-stage spermatids and others with abnormal leaf shapes (arrowheads) that likely carry the Y chromosome. In *dcr-2* (O) and *ago2* (P) mutants, cysts are disorganized, spermatid nuclei are abnormally shaped and scattered in the testis, and histones remain associated. Scale bars represent 10  $\mu$ m; note scale of (N) is enlarged relative to (M), (O), and (P).

(Q–T) Seminal vesicles. In control males (Q), the seminal vesicle is filled with sperm as revealed by the presence of needle-shape nuclei. (R) *nmy* exhibits reduced seminal vesicle contents. In contrast, seminal vesicles in *dcr-2* (S) and *ago2* (T) mutants are empty and only the round nuclei of the seminal vesicle walls are seen, indicating that no mature sperm are generated. Scale bar represents 10  $\mu$ m. See also Figure S7.

suggested. More importantly, they strongly support the scenario that multiple hpRNAs (i.e., *Nmy* and *Tmy*) provide overlapping defense against both distorter loci during SR control.

Overall, our molecular analysis of the Winters and Durham systems reveal striking biological utilizations and functional necessities for RNAi in the control of intragenomic conflict, especially given (1) how rapidly evolving these SR distorter systems are, and (2) how potent the consequences of loss of hpRNA-mediated control are in terms of population extinction.

## DISCUSSION

This study provides critical linkages among the RNAi pathway, hpRNA biogenesis and function, and suppression of SR bias. The evolutionary behavior of SR systems conforms to a “Red Queen” effect (Van Valen, 1973) (Figure 7A), in which a seemingly

static outcome (equal transmission of X and Y sperm) actually involves intense, opposing and rapidly evolving genetic programs (Figure 7B). Our studies provide striking evidence that endogenous RNAi is a central molecular pathway that resolves SR distortion and may potentially have an impact on hybrid sterility. We provide molecular and genetic evidence of a potential hierarchy, in that *Dox* is a prime direct target of *Nmy* based on the observation that it supplies the majority of targeting siRNAs. Nevertheless, *Tmy* provides a secondary defense: since *Tmy* exhibits extensive complementarity to *Dox* that is non-overlapping with *Nmy*, *Tmy* siRNAs maintain targeting to *Dox* even in *nmy* mutants. *Tmy* can directly repress *Dox* in sensor assays, and most importantly, RNAi mutants exhibit strongly elevated *Dox* transcripts in testis, consistent with co-targeting endogenous action of both hpRNAs on *Dox*. Moreover, we show these principles to be true for *MDox*, strongly implying this locus as a

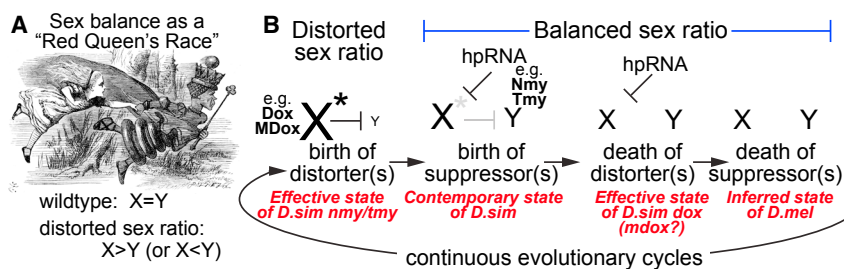


**Figure 7. Continuous Cycles of Sex-Ratio Distortion and Suppression via the hpRNA/RNAi Pathway Mediate Balanced Sex Ratio**

(A) A John Tenniel illustration from Lewis Carroll's *Through the Looking-Glass*, where the Red Queen says to Alice, "Now, here, you see, it takes all the running you can do, to keep in the same place." Leigh Van Valen proposed this as a metaphor for co-evolution system, which can be extended to a rapidly evolving genomic conflict, or arms-race scenario, where the net outcome is to maintain the status quo.

(B) In the case of this study, the seemingly static outcome of equal male and female progeny is driven by an intense battle between the sex chromosomes, in which the X continually attempts to gain an advantage over the Y via *de novo* meiotic X-linked distorter factors (designated by the asterisk, e.g., *Dox* and *MDox*). The dramatic loss of Y transmission creates a strong pressure to innovate suppressors, which we have shown to be hpRNA loci that function via the RNAi pathway (e.g., *Nmy* and *Tmy*). In general, all known *Drosophila* hpRNAs are evolutionarily young, and, consistent with this model, their action is only needed as long as the distorters are active. Once the distorter is inactivated, there is no selective pressure to maintain the hpRNA. Note that multiple cycles of distortion and suppression may occur in parallel.

functional distorter. Overall, we reveal that multiple evolutionary nascent hpRNAs (*Nmy/Tmy*) are individually required for species preservation via suppression of Winters and Durham SR (*Dox/MDox*) distorters in *D. simulans* (Figure 7B).

In the future, further dissection of the genetic contributions of the individual hpRNAs and distorters will shed light on their relative contributions to Winters and Durham SR systems and the extent to which they are distinct systems or partially overlapping as indicated by our studies. This will be a challenge in a non-model fly that lacks the genetic tools available in *D. melanogaster* but will be important to understand how these newly emerging factors are endowed with such powerful activities. For example, compelling hypotheses to test include whether specific deletions of the *Tmy* hairpin alone can recapitulate SR bias, whether *Tmy* exhibits derepression of other distorter factors, and whether *nmy/tmy* double mutant might exhibit only SR or may prove to recapitulate sterility found in RNAi mutants. Thus far, *Nmy* and *Tmy* loci have proven recalcitrant to repeated attempts for CRISPR/Cas9 targeting, and it is not clear whether something about their repeat structure affects this endeavor. Moreover, the close linkage of these loci will be a challenge for any efforts to generate recombinants. Still, it will be worthwhile to pursue the generation of new genetic tools.

Remarkably, there is a third SR distortion system in *D. simulans* ("Paris"). While it is genetically complex, it was recently shown to depend on HP1D2, a recently evolved paralog of the piRNA factor Rhino (Helleu et al., 2016). Thus, there are apparently molecular linkages of SR systems with small RNA systems, on both driving and suppressing sides. Although the mechanism of Paris SR remains to be determined, HP1D2 protein localizes to the heterochromatic Y chromosome, which provides a connection to the observation that driving Paris alleles prevent segregation of Y chromatids during meiosis II (Helleu et al., 2016). On the other hand, the defect in Winters SR appears to be post-meiotic (Tao et al., 2007a, 2007b), indicating mechanistic diversity in how depletion of male sperm might be achieved by *de novo* genes.

On the other hand, the sister species *D. melanogaster* appears to lack SR systems, testament to the extremely rapid rise and fall of SR systems during evolution. The adaptive properties of hpRNAs make them ideal genetic elements to tame such selfish

meiotic drive elements, which are theorized to be under constant cycles of emergence, suppression, and disappearance (Jaenike, 2008; Willis, 2009). There is mounting evidence that genetic systems that manifest in SR defects are often associated with sterility (Phadnis and Orr, 2009; Zhang et al., 2015). Our findings support the notion that the success or failure to resolve intragenomic conflicts using RNAi would be intimately connected to speciation.

While these roles were unexpected in light of the fact that metazoan RNAi biology has been so challenging to appreciate, the situation would have been different had a species only slightly diverged from *D. melanogaster* initially been selected as a genetic model. This parallels the inference that RNAi might have been recognized earlier had certain budding yeasts other than *Saccharomyces cerevisiae* been studied earlier (Drinnenberg et al., 2009). Indeed, functional studies across a broader phylogeny will be necessary to appreciate the evolving requirements of small RNA regulation, beyond standard model organisms (Sarkies et al., 2015). The availability of our *D. simulans* RNAi mutants opens the door to molecular identification of novel selfish genetic elements that induce SR bias and/or hybrid sterility, in both the Winters and Durham systems.

## STAR★METHODS

Detailed methods are provided in the online version of this paper and include the following:

- KEY RESOURCES TABLE
- CONTACT FOR REAGENT AND RESOURCE SHARING
- EXPERIMENTAL MODEL AND SUBJECT DETAILS
  - *Drosophila simulans*
  - Cell Lines
- METHOD DETAILS
  - Fertility and Sex Ratio Tests
  - Small RNA Library Preparation
  - Small RNA Analysis
  - Total RNA Library Preparation
  - RNA-Seq Analysis
  - Generation of hpRNA Expression Constructs
  - β-Elimination Test

- Argonaute Immunoprecipitations
- Small RNA Northern Blotting
- Luciferase Sensor Assays
- CRISPR/Cas9 Mutagenesis of *D. simulans*
- qPCR
- Testis Cytology
- QUANTIFICATION AND STATISTICAL ANALYSIS
- DATA AND SOFTWARE AVAILABILITY

## SUPPLEMENTAL INFORMATION

Supplemental Information includes seven figures and two tables and can be found with this article online at <https://doi.org/10.1016/j.devcel.2018.07.004>.

## ACKNOWLEDGMENTS

We are grateful to Yun Tao for discussion and members of the *simulans* clade PacBio sequencing consortium (J.J. Emerson, Amanda Larracuente, Colin Meiklejohn, and Kristi Montooth) for access to *Drosophila simulans* PacBio data in the *Tmy* region. We thank Zhigang Jin, Lijuan Kan, Alex Flynt, and Rui Gao for helping to prepare *D. simulans* samples and Nicolas Robine for initial analysis of small RNA data. We thank Masatoshi Yamamoto and San Diego Drosophila Stock Center for fly stocks. Work in B.L.’s group was supported by a grant to R.D. from the Agence National de la Recherche (ANR-16-CE12-0006-01). Work in E.C.L.’s group was supported by the National Institutes of Health (R01-NS083833 and R01-GM083300), BSF-2015398, and MSK Core Grant P30-CA008748.

## AUTHOR CONTRIBUTIONS

C.J.L. and F.H. performed the molecular and genetic analyses. F.H. performed the *D. simulans* CRISPR mutagenesis. R.D. analyzed testis cytology in mutants. J.V. and J.W. performed computational analyses. P.S. generated constructs and initiated the project. B.L. and E.C.L. supervised analysis and interpreted results, and E.C.L. wrote the manuscript with input from co-authors.

## DECLARATION OF INTERESTS

The authors declare no competing interests.

Received: April 27, 2018

Revised: June 13, 2018

Accepted: July 2, 2018

Published: August 6, 2018

## REFERENCES

- Chung, W.J., Okamura, K., Martin, R., and Lai, E.C. (2008). Endogenous RNA interference provides a somatic defense against *Drosophila* transposons. *Curr. Biol.* **18**, 795–802.
- Czech, B., Malone, C.D., Zhou, R., Stark, A., Schlingeheyde, C., Dus, M., Perrimon, N., Kellis, M., Wohlschlegel, J.A., Sachidanandam, R., et al. (2008). An endogenous small interfering RNA pathway in *Drosophila*. *Nature* **453**, 798–802.
- Drinnenberg, I.A., Weinberg, D.E., Xie, K.T., Mower, J.P., Wolfe, K.H., Fink, G.R., and Bartel, D.P. (2009). RNAi in budding yeast. *Science* **326**, 544–550.
- Dubruille, R., and Loppin, B. (2015). Protection of *Drosophila* chromosome ends through minimal telomere capping. *J. Cell Sci.* **128**, 1969–1981.
- Ghildiyal, M., Seitz, H., Horwich, M.D., Li, C., Du, T., Lee, S., Xu, J., Kittler, E.L., Zapp, M.L., Weng, Z., et al. (2008). Endogenous siRNAs derived from transposons and mRNAs in *drosophila* somatic cells. *Science* **320**, 1077–1081.
- Haley, B., and Zamore, P.D. (2004). Kinetic analysis of the RNAi enzyme complex. *Nat. Struct. Mol. Biol.* **11**, 599–606.
- Helleu, Q., Gérard, P.R., Dubruille, R., Ogereau, D., Prud'homme, B., Loppin, B., and Montchamp-Moreau, C. (2016). Rapid evolution of a Y-chromosome heterochromatin protein underlies sex chromosome meiotic drive. *Proc. Natl. Acad. Sci. USA* **113**, 4110–4115.
- Jaenike, J. (2008). X chromosome drive. *Curr. Biol.* **18**, R508–R511.
- Kawamura, Y., Saito, K., Kin, T., Ono, Y., Asai, K., Sunohara, T., Okada, T.N., Siomi, M.C., and Siomi, H. (2008). *Drosophila* endogenous small RNAs bind to Argonaute2 in somatic cells. *Nature* **453**, 793–797.
- Kim, D., Langmead, B., and Salzberg, S.L. (2015). HISAT: a fast spliced aligner with low memory requirements. *Nat. Methods* **12**, 357–360.
- Kingan, S.B., Garrigan, D., and Hartl, D.L. (2010). Recurrent selection on the winters sex-ratio genes in *Drosophila simulans*. *Genetics* **184**, 253–265.
- Ku, H.Y., Gangaraju, V.K., Qi, H., Liu, N., and Lin, H. (2016). Tudor-sn interacts with Piwi antagonistically in regulating spermatogenesis but synergistically in silencing transposons in *drosophila*. *PLoS Genet.* **12**, e1005813.
- Langmead, B., and Salzberg, S.L. (2012). Fast gapped-read alignment with Bowtie 2. *Nat. Methods* **9**, 357–359.
- Langmead, B., Trapnell, C., Pop, M., and Salzberg, S.L. (2009). Ultrafast and memory-efficient alignment of short DNA sequences to the human genome. *Genome Biol.* **10**, R25.
- Lee, J.E., and Yi, R. (2014). Highly efficient ligation of small RNA molecules for microRNA quantitation by high-throughput sequencing. *J. Vis. Exp.* **18**, e52095.
- Liao, Y., Smyth, G.K., and Shi, W. (2014). featureCounts: an efficient general purpose program for assigning sequence reads to genomic features. *Bioinformatics* **30**, 923–930.
- Love, M.I., Huber, W., and Anders, S. (2014). Moderated estimation of fold change and dispersion for RNA-seq data with DESeq2. *Genome Biol.* **15**, 550.
- Lu, R., Maduro, M., Li, F., Li, H.W., Broitman-Maduro, G., Li, W.X., and Ding, S.W. (2005). Animal virus replication and RNAi-mediated antiviral silencing in *Caenorhabditis elegans*. *Nature* **436**, 1040–1043.
- Lucchetta, E.M., Carthew, R.W., and Ismagilov, R.F. (2009). The endo-siRNA pathway is essential for robust development of the *Drosophila* embryo. *PLoS One* **4**, e7576.
- Neph, S., Kuehn, M.S., Reynolds, A.P., Haugen, E., Thurman, R.E., Johnson, A.K., Rynes, E., Maurano, M.T., Vierstra, J., Thomas, S., et al. (2012). BEDOPS: high-performance genomic feature operations. *Bioinformatics* **28**, 1919–1920.
- Okamura, K., Chung, W.J., Ruby, J.G., Guo, H., Bartel, D.P., and Lai, E.C. (2008). The *Drosophila* hairpin RNA pathway generates endogenous short interfering RNAs. *Nature* **453**, 803–806.
- Okamura, K., and Lai, E.C. (2008). Endogenous small interfering RNAs in animals. *Nat. Rev. Mol. Cell. Biol.* **9**, 673–678.
- Okamura, K., Liu, N., and Lai, E.C. (2009). Distinct mechanisms for microRNA strand selection by *Drosophila* Argonautes. *Mol. Cell* **36**, 431–444.
- Phadnis, N., and Orr, H.A. (2009). A single gene causes both male sterility and segregation distortion in *Drosophila* hybrids. *Science* **323**, 376–379.
- Quinlan, A.R., and Hall, I.M. (2010). BEDTools: a flexible suite of utilities for comparing genomic features. *Bioinformatics* **26**, 841–842.
- Sarkies, P., Selkirk, M.E., Jones, J.T., Blok, V., Boothby, T., Goldstein, B., Hanelt, B., Ardila-Garcia, A., Fast, N.M., Schiffer, P.M., et al. (2015). Ancient and novel small RNA pathways compensate for the loss of piRNAs in multiple independent nematode lineages. *PLoS Biol.* **13**, e1002061.
- Tao, Y., Araripe, L., Kingan, S.B., Ke, Y., Xiao, H., and Hartl, D.L. (2007a). A sex-ratio meiotic drive system in *Drosophila simulans*. II: an X-linked distorter. *PLoS Biol.* **5**, e293.
- Tao, Y., Hartl, D.L., and Laurie, C.C. (2001). Sex-ratio segregation distortion associated with reproductive isolation in *Drosophila*. *Proc. Natl. Acad. Sci. USA* **98**, 13183–13188.
- Tao, Y., Masly, J.P., Araripe, L., Ke, Y., and Hartl, D.L. (2007b). A sex-ratio meiotic drive system in *Drosophila simulans*. I: an autosomal suppressor. *PLoS Biol.* **5**, e292.
- Van Valen, L. (1973). A new evolutionary law. *Evol. Theory* **1**, 1–30.
- Wang, L., Wang, S., and Li, W. (2012). RSeQC: quality control of RNA-seq experiments. *Bioinformatics* **28**, 2184–2185.

- Wang, X.H., Aliyari, R., Li, W.X., Li, H.W., Kim, K., Carthew, R., Atkinson, P., and Ding, S.W. (2006). RNA interference directs innate immunity against viruses in adult *Drosophila*. *Science* 312, 452–454.
- Wen, J., Duan, H., Bejarano, F., Okamura, K., Fabian, L., Brill, J.A., Bortolamiol-Becet, D., Martin, R., Ruby, J.G., and Lai, E.C. (2015). Adaptive regulation of testis gene expression and control of male fertility by the *Drosophila* hairpin RNA pathway. *Mol. Cell* 57, 165–178.
- Willis, J.H. (2009). Genetics. Origin of species in overdrive. *Science* 323, 350–351.
- Yasuno, Y., Inoue, Y.H., and Yamamoto, M.T. (2013). Elimination of Y chromosome-bearing spermatids during spermiogenesis in an autosomal sex-ratio mutant of *Drosophila simulans*. *Genes Genet. Syst* 88, 113–126.
- Zhang, L., Sun, T., Woldesellassie, F., Xiao, H., and Tao, Y. (2015). Sex ratio meiotic drive as a plausible evolutionary mechanism for hybrid male sterility. *PLoS Genet.* 11, e1005073.

## STAR★METHODS

## KEY RESOURCES TABLE

REAGENT or RESOURCE	SOURCE	IDENTIFIER
<b>Antibodies</b>		
Monoclonal ANTI-FLAG® M2 antibody	SIGMA-ALDRICH	Cat#F1804
Anti-Ago1 antibody	abcam	Cat#ab5070
Anti-Histone Antibody, Pan, clone F152.C25.WJJ	Millipore	Cat#MABE71
Monoclonal Anti- $\alpha$ -Tubulin antibody produced in mouse	SIGMA-ALDRICH	Cat#T9026
Alexa Fluor® 488 AffiniPure Goat Anti-Mouse IgG, Fc $\gamma$ Subclass 1 Specific	Jackson ImmunoResearch	Cat#115-545-205
Alexa Fluor® 594 AffiniPure Goat Anti-Mouse IgG, Fc $\gamma$ Subclass 2a Specific	Jackson ImmunoResearch	Cat#115-585-206
DyLight™ 488 Goat anti-Mouse IgG (H&L)	ThermoFisher	Cat#35502
<b>Bacterial and Virus Strains</b>		
NEB® Stable Competent <i>E. coli</i>	NEB	C3040I
<b>Chemicals, Peptides, and Recombinant Proteins</b>		
Alexa Fluor™ 633 Phalloidin	ThermoFisher	Cat#A22284
<b>Critical Commercial Assays</b>		
TRIzol	Invitrogen	Cat#15596-018
Adenylation Kit	NEB	Cat#E2610L
T4 RNA ligase 1	NEB	Cat#M0204L
T4 RNA ligase 2 (1-249; K227Q)	NEB	Cat#M0351L
Superscript III RT kit	Invitrogen	Cat#18080-051
GeneScreen Plus membrane	PerkinElmer	Cat#NEF1017001PK
SequaGel UreaGel System	National Diagnostics	Cat#EC-833
T4 PNK	NEB	Cat#M0201L
ATP, [gamma-P32]	PerkinElmer	Cat#BLU502Z250UC
Dynabeads protein G	Life Technologies	Cat#10004D
T4 DNA ligase	NEB	N/A
Effectene Transfection Reagent	QIAGEN	Cat#301427
Illumina Truseq Total RNA library Prep Kit LT	illumina	Cat#RS-122-2202
TruSeq RNA Single Indexes Set A	illumina	Cat#20020492
TruSeq RNA Single Indexes Set B	illumina	Cat#20020493
RNaseOUT	invitrogen	Cat#10777-019
TURBO DNA-free™ Kit	Ambion	Cat#AM1907
<b>Deposited Data</b>		
wXD1 sRNA	This study	NCBI Short Read Archive (SRA) portal, BioProject ID SRA: PRJNA477366
12-2-7 sRNA	This study	NCBI Short Read Archive (SRA) portal, BioProject ID SRA: PRJNA477366
wXD1 RNA-seq	This study	NCBI Short Read Archive (SRA) portal, BioProject ID SRA: PRJNA477366
<b>Experimental Models: Cell Lines</b>		
<i>D. melanogaster</i> cell line: S2R+	DGRC	Flybase: FBtc0000150
<i>D. melanogaster</i> cell line: Flag-HA-Ago2 stable S2R+	Eric Lai lab	N/A
<b>Experimental Models: Organisms/Strains</b>		
<i>D. simulans</i> w[XD1]	BestGene Inc.	N/A
<i>D. simulans</i> e exf p	Yasuno et al. (2013)	N/A

(Continued on next page)

**Continued**

REAGENT or RESOURCE	SOURCE	IDENTIFIER
<i>D. simulans</i> 12-2-7	Tao et al. (2007b)	N/A
<i>D. simulans</i> 5-2	Tao et al. (2007b)	N/A
<i>D. simulans dcr-2[DsRed]</i>	This study	N/A
<i>D. simulans ago2[DsRed]</i>	This study	N/A
Oligonucleotides		
Refer to Table S2	This study	N/A
Recombinant DNA		
pUAS-DsRed-Nmy	This study	N/A
pUAS-DsRed-nmy	This study	N/A
pUAS-DsRed-Tmy	This study	N/A
pUAS-DsRed-tmy	This study	N/A
psiCHECK-Dox	This study	N/A
psiCHECK-MDox	This study	N/A
pHD-3XDsRed-dcr-2 HRD	This study	N/A
pHD-3XDsRed-ago2 HRD	This study	N/A
pDCC6-dcr-2-sgRNA1	This study	N/A
pDCC6-dcr-2-sgRNA2	This study	N/A
pDCC6-dcr-2-sgRNA3	This study	N/A
pDCC6-ago2-sgRNA3	This study	N/A
pDCC6-ago2-sgRNA5	This study	N/A
Software and Algorithms		
Bowtie2 v2.3.0	Langmead and Salzberg (2012)	<a href="http://bowtie-bio.sourceforge.net/bowtie2/index.shtml">http://bowtie-bio.sourceforge.net/bowtie2/index.shtml</a>
Bowtie v1.2	Langmead et al. (2009)	<a href="http://bowtie-bio.sourceforge.net/">http://bowtie-bio.sourceforge.net/</a>
Hisat2 v2.0.5	Kim et al. (2015)	<a href="https://ccb.jhu.edu/software/hisat2/index.shtml">https://ccb.jhu.edu/software/hisat2/index.shtml</a>
R	R Core Team, 2013	<a href="http://www.R-project.org/">http://www.R-project.org/</a>
BEDtools	Quinlan and Hall, (2010)	<a href="http://bedtools.readthedocs.io/">http://bedtools.readthedocs.io/</a>
BEDops	Neph et al. (2012)	<a href="https://bedops.readthedocs.io">https://bedops.readthedocs.io</a>
FASTXtoolkit		<a href="http://hannonlab.cshl.edu/fastx_toolkit/">http://hannonlab.cshl.edu/fastx_toolkit/</a>

**CONTACT FOR REAGENT AND RESOURCE SHARING**

Further information and requests for resources and reagents should be directed to and will be fulfilled by the Lead Contact, Eric C. Lai ([laie@mskcc.org](mailto:laie@mskcc.org)).

**EXPERIMENTAL MODEL AND SUBJECT DETAILS*****Drosophila simulans***

*w[XD1]* was obtained from Bestgene, Inc. and used as the control strain for all the analyses in the paper. For *nmy* mutants, *SR12-2-7* and *nmy[5-2]* were provided by Yun Tao and *e exf p* by Masatoshi Yamamoto. RNAi mutants, *dcr-2* and *ago2* are generated as described below in the main **STAR Methods** text. All stocks were maintained at 18°C or 25°C, as described.

**Cell Lines**

We acquired S2R+ from DGRC and the cells were maintained at 25°C in Schneider's medium containing 10% FBS.

**METHOD DETAILS****Fertility and Sex Ratio Tests**

To obtain males for the assay, bottles were set up at 25°C to collect eggs of indicated genotypes for 2 days and transferred to 18°C until adult flies emerged. 5-day-old individual males were mated to *w[XD1]* virgins and 5-day-old individual females were mated to

3 w[XD1] males. All vials were raised in 18°C and flipped every other day for 2 weeks. Progeny from 7 vials were counted for data analysis.

### Small RNA Library Preparation

For small RNA analysis, we extracted RNA from testes and accessory glands of 7-day-old *D. simulans* w[XD1] and *nmy* mutants using Trizol (Invitrogen). 1 µg of total RNA were used to prepare small RNA libraries largely as previously described (Lee and Yi, 2014). Adenylation of 3' linker was performed in a 40 µL reaction at 65°C for 1 hr containing 200 pmol 3' linker, 1X 5' DNA adenylation reaction buffer, 100 nM ATP and 200 pmol Mth RNA ligase and the reaction is terminated by heated to 85°C for 5 min. Adenylated 3' linker was then precipitated using ethanol and was used for 3' ligation reaction containing 10% PEG8000, 1X RNA ligase buffer, 20 µM adenylated 3' linker and 100 U T4 RNA Ligase 2 truncated K227Q. The 3' ligation reaction was performed at 4°C for overnight and the product were purified using 15% Urea-PAGE gel. The small RNA-3' linker hybrid was then subjected to 5' ligation reaction at 37°C for 4 hr containing 20% PEG8000, 1X RNA ligase buffer, 1 mM ATP, 10 µM RNA oligo, 20 U RNaseOUT and 5 U T4 RNA ligase 1. cDNA synthesis reaction was then proceeded immediately by adding following components to the ligated product: 2 µl 5x RT buffer, 0.75 µl 100 mM DTT, 1 µl 1 µM Illumina RT Primer, and 0.5 µl 10 mM dNTPs. The RT mix was incubated at 65°C for 5 min and cooled to room temperature and transfer on to ice. 0.5 µL of superscript III RT enzyme and 0.5 µL RNase OUT were added to the RT mix and the reaction was carried out at 50°C for 1 hr. cDNA libraries were amplified using 15 cycles of PCR with forward and Illumina index reverse primers and the amplified libraries were purified by 8% non-denaturing acrylamide gel. Purified libraries were sequenced on HiSeq2500 using SR50 at the New York Genome Center. Oligo sequences and reagents used for library preparation are provided in [Table S2](#) and [Key Resources Table](#), respectively.

### Small RNA Analysis

We aggregated small RNA libraries data mentioned above with other public datasets ([Table S1](#)). sRNA reads generated in this study were processed as follows: Raw sequence reads were adapter trimmed using fastx toolkit (fastx\_clipper -a TGGAATTCTCGGGT -Q 33 -i library\_name.fastq). After filtering <15 nt reads using a custom shell script, we mapped the data to both *D. simulans* r2.02 from Flybase and PacBio contigs using the Bowtie2 software (very-sensitive-local; -D 20 -R 3 -N 0 -L 20 -i S,1,0,50). We mapped >15nt sRNAs to both r2.02 and PacBio assembly and normalized them per million mapped miRNAs from the respective libraries. The resulting small RNA alignments in SAM format were converted to BED for downstream processing using the BEDops software. To identify small RNA mappings with up to 3 mismatches, either at any positions or by requiring continuous matching to nucleotide positions 1 and > 13 (no mismatches allowed in the seed region 2-13nt), small RNA alignment SAM files from bowtie mapping (with -v3 –best –strata options) were filtered using a custom shell script and converted to BED format for downstream processing and visualization. For public small RNA datasets described in this study, the data was mapped using Bowtie (with –v0 –best –strata options) to Pacbio assembly and the reads were normalized to million reads in their respective libraries.

### Total RNA Library Preparation

We extracted RNA from testes (dissected free of accessory glands) of 7-day-old *D. simulans* w[XD1] flies using Trizol (Invitrogen). Illumina Truseq Total RNA library Prep Kit LT was used to make stranded RNA-seq libraries from 650 ng of total RNA. Manufacturer's protocol was followed except for using 8 cycles of PCR to amplify the final library instead of the recommended 15 cycles, to minimize artifacts caused by PCR amplification. All samples were pooled together using the barcoded adapters provided by the manufacturer and the sequencing was performed by HiSeq2500 instrument using PE75 at the New York Genome Center.

### RNA-Seq Analysis

We supplemented our RNA-seq data with analysis of publicly available *D. simulans* RNA-seq data from various tissues ([Table S1](#)). The data was mapped to both *D. simulans* r2.02 and PacBio contigs using hisat2 aligner with default parameters. For annotated gene models available from FlyBase release r2.02, we obtained strand-specific mapped read counts using the featureCounts software (Liao et al., 2014). The read counts were normalized to FPKM using the DEseq2 package in R (Love et al., 2014). As genomic sequences of hpRNAs *nmy* and *tmy* were not assembled properly in r2.02, we quantified their expression using PacBio mappings. To visualize RNA-seq mapping in the IGV genome browser, we converted the sequence alignments in bam format to UCSC BigWig format using the BamToWig.py tool in the RSeqQC package (Wang et al., 2012).

### Generation of hpRNA Expression Constructs

*Nmy* and *nmy* (mutant) expression constructs were cloned from w[XD1] and 12-2-7 strains, respectively, into the 3' UTR site of pUAST-DsRed. For *Tmy* construct, the left arm and right arm fragments were amplified separately from w[XD1] genomic DNA, and then three-way ligation was performed to clone both arms into the 3' UTR site of pUAST-DsRed. To avoid recombination, the *pUAST-DsRed-Tmy* construct was transformed into NEB stable competent cells. The primers used for cloning are listed in [Table S2](#).

### B-Elimination Test

To analyze small RNA 3' termini, S2R+ cells were transfected with *UAS-Tmy*, *UAS-Nmy* or *UAS-nmy* constructs using Effectene transfection reagent (QIAGEN) for 3 days and total RNAs were extracted using Trizol. RNAs were then treated with sodium periodate

in borax/boric-acid buffer followed by sodium hydroxide treatment, and Northern blotting analysis as described (Okamura et al., 2008). Probes for blotting are listed in [Table S2](#).

### Argonaute Immunoprecipitations

To analyze Argonaute loading, we transfected hpRNA constructs into FLAG-HA-AGO2 stable S2R+ cell using Effectene transfection reagent (QIAGEN) for 3 days. We then followed the IP protocol described in (Okamura et al., 2009). Briefly, after washing with PBS,  $10^7$  cells were lysed with 500  $\mu$ L of Ago IP buffer (30 mM HEPES pH7.5, 150 mM KOAc, 2 mM Mg(OAc)<sub>2</sub>, 5 mM DTT, 0.1% NP40, 1X Protease Inhibitor(Roche) and 20U RNaseOUT). Cleared cell lysates were first incubated with Flag-M2-conjugated beads and supernatant from the first IP was then used for AGO1-IP. Beads were washed five times using lysis buffer. Bound RNA was extracted from beads using Trizol, and was analyzed by small RNA Northern blotting describing below.

### Small RNA Northern Blotting

RNA was run on 15% urea acrylamide gel (SequaGel UreaGel System, National Diagnostics) in 1X TBE buffer, and transferred to GeneScreen Plus membrane (Perkin Elmer) in 0.5X TBE buffer for 1 hr. After UV-crosslinking, the membrane was incubated with pre-hyb buffer for 1 hr and was hybridized with gamma-P<sup>32</sup> labeled probes for overnight at 50°C. Probe sequences are listed in [Table S2](#).

### Luciferase Sensor Assays

Dox and MDox sequences were amplified from *w[XD1]* into psiCHECK luciferase sensors. All the primers used for cloning are listed in [Table S2](#). Other hpRNA constructs were described previously (Okamura et al., 2008). To perform sensor assays,  $10^5$  S2 cells were seeded per well of 96-well plate and transfected with 25 ng UAS-DsRed or UAS-DsRed hairpin constructs, 50 ng psiCHECK sensors and 12.5 ng Ub-Gal4. Luciferases were measured 3 days after transfection using Dual Glo luciferase assay system (Promega) and Cytaion5 (BioTek). The fold repression values were normalized to empty psiCHECK and UAS-DsRed group. Individual tests were done in quadruplicate and the averaged values from three biological replicate samples were subjected to statistical analysis.

### CRISPR/Cas9 Mutagenesis of *D. simulans*

sgRNAs were designed using <http://flycrispr.molbio.wisc.edu/>, and were designed to delete most of the target gene and replace it with a 3xP3:DsRed marker. sgRNA oligo pairs were phosphorylated by T4 PNK (NEB), annealed and ligated into BbsI digested pDCC6 vector using T4 DNA ligase (NEB). Homology arms of *ago2* and *dcr-2* were amplified from genomic DNA and cloned into pH-DsRed-attp; two different donor arm combinations were used for *dcr-2* to generate *dcr-2-1* and *dcr-2-2* alleles. All primers used to clone sgRNAs, validate sgRNA target sites, and clone donor constructs are listed in [Table S2](#).

100 ng/ $\mu$ L of pDCC6-sgRNA constructs and 100 ng/ $\mu$ L donor plasmid were mixed for injection into *D. simulans w[XD1]* embryos (BestGene Inc, Chino Hills). Flies were cultured on standard cornmeal food at 25°C. To score for germline mutations, G0 adult flies were crossed to *w[XD1]* flies and F1 progeny were screened for DsRed+ eyes under a Leica fluorescent microscope. Primers used to screen for on-target hybrid PCR products on the left and right flanks at *ago2* and *dcr-2* are listed in [Table S2](#), as are primer pairs to validate deletion of internal gene segments at each locus in homozygous mutants.

### qPCR

Because *D. simulans* lacks balancer chromosomes, and the 3xP3:DsRed marker was not completely reliable for identifying homozygous mutants, we found it was necessary to genotype flies to confirm mutants prior to pooling RNA samples for further analysis. Therefore, we collected 7-day-old putative *dcr-2* or *ago2* mutant males based on DsRed eye intensity, and dissected their reproductive systems (testis and accessory gland) into PBS. We genotyped their respective thoraces, and prepared total RNA from combined, confirmed, mutant reproductive systems using Trizol (Invitrogen) and DNase treatment using TURBO DNA-free™ kit (Ambion). cDNA was synthesized using SuperScript III First-Strand Synthesis System with random primers (Invitrogen). qPCR reactions were performed with CFX96 Touch™ Real-Time PCR Detection System (Bio-Rad). Primers for *Dox*, *MDox* and control *Rp32* are listed in [Table S2](#).

### Testis Cytology

For each mutant genotype, 0-4 day old DsRed positive males were dissected and the mutant testes were recognized with the empty seminal vesicle and disrupted spermatogenesis. Whole-mount testes were stained as described (Dubrulle and Loppin, 2015). Briefly, testes were dissected in PBS-T (1X PBS with 0.15% Triton), fixed in 4% formaldehyde 1X PBS for 20 min, washed 3 times in PBS-T before 4°C overnight incubation in primary antibodies. Primary antibodies were mouse IgG2a monoclonal anti-pan-histone, clone F152 (1:1000; Millipore), mouse IgG1 anti-alpha-tubulin clone DM1A (1:1000; Sigma-Aldrich). Then, they were washed 3 times for 20 min in PBS-T prior to incubation with secondary antibodies for 2-3 hours at room temperature. We used Alexa Fluor-coupled goat anti-mouse IgG1 and IgG2a (1:1,000; Jackson ImmunoResearch). Samples were then washed 3 times for 20 min in PBS-T before mounting.

For F-actin staining, testes were incubated in phalloidin-fluoroprobe (Interchim) diluted in 1X-PBS (1:100) and incubated at room temperature for 30 min. Testes were then washed again and incubated for 30 min at 37°C in 2mg/mL RNase A, rinsed and mounted in mounting medium containing 5  $\mu$ g/mL propidium iodide (Sigma-Aldrich) to stain DNA. For other stainings, DNA was stained by directly mounting tissues in mounting medium (Dako) containing 10  $\mu$ g/mL DAPI (Sigma-Aldrich).

Images were acquired on a LSM800 confocal microscope (Carl Zeiss) using the Zen software in .czi format then converted to .tiff using Zen Digital Imaging or FIJI software.

#### **QUANTIFICATION AND STATISTICAL ANALYSIS**

To evaluate statistical significance for sensor assays and qPCR tests, we used unpaired Student's *t*-test to calculate p-values. The error bars shown in fertility assay represent standard error (SEM), and standard deviation (SD) in sensor assays and qPCR tests.

#### **DATA AND SOFTWARE AVAILABILITY**

All of the raw small RNA and RNA-seq data reported in this study were deposited in the NCBI Short Read Archive (SRA) portal under the BioProject ID SRA: PRJNA477366.